Synthesis, Characterization of CuPp-TiO_2 Photocatalyst and the Photodegradation Study for 4-Nitrophenol

School : Xi'an Gaoxin No.1 High School

Location: Xi'an, Shaanxi, China

Counselor: Qingxiang Hui

Member: Qihua Wang Zonglin Li Yifan Zhao

XI`AN GAOXIN
NO.1 HIGH SCHOOL

Synthesis, Characterization of CuPp-TiO_2 Photocatalyst and the Photodegradation Study for 4-Nitrophenol

Abstract:

A novel copper porphyrin (CuPp), utilized for TiO_2 modification, was designed, synthesized and characterized spectroscopically. A TiO_2 composite photocatalyst based on CuPp, namely CuPp-TiO_2, was obtained by the solvothermal method and investigated by means of spectroscopic measurements. A nitrogen adsorption–desorption test has verified the mesoporous structure for CuPp-TiO_2, which results in a moderate N_2 adsorbing capacity. The tests of prepared CuPp-TiO_2 have shown high photocatalytic activity and stability in the degradation of 4-nitrophenol (4-NP).

Keywords: photocatalysis, Cu(II) porphyrin, TiO_2, photodegradation, 4-nitrophenol

Statement of Originality

The research process and result of this team are conducted and derived under the guidance of the instructor. Other than the referenced content and the acknowledged sources, this paper does not include any published findings by this group or any other researchers. If there is any inaccuracy, this team is accountable for the all liabilities.

Signature:

Date:

Synthesis, Characterization of CuPp-TiO_2 Photocatalyst and the Photodegradation Study for 4-Nitrophenol

1. Introduction

In recent years, the problem of environmental pollution has become a major challenge for humanity [1, 2]. The organic pollutants in the water severely threaten the health of human beings. TiO_2 is widely used as a photocatalyst in degrading pollutants in the water because of its low toxicity, chemical stability, and high photocatalytic activity [3-6]. However, its use of solar energy is limited by the wide band-gap of TiO_2 (Eg = 3.2 eV for anatase) which can only absorb UV light [7, 8]. Some methods have been used to solve this issue including doping, deposition, semiconductor coupling and dye sensitization [9, 10]. Among these, the dye sensitization has aroused public's interest for its high efficiency and good thermal stability.

Porphyrins are a kind of compound to be recognized as the most promising sensitizers, which can be employed in dye sensitization [11-13]. In particular, metal porphyrins have been shown to be efficient photosensitizers and catalysts for degradation. It has been demonstrated that Cu(II) porphyrin has an enhanced photocatalytic activity in sensitizing TiO_2 for the decomposition of organic pollutants [14,15]. Therefore, a novel copper porphyrin has been designed and synthesized, as well as its corresponding TiO_2 composite photocatalyst CuPp-TiO_2, which was prepared by the solvothermal method and characterized with various spectroscopic technologies. The prepared CuPp-TiO_2 photocatalyst is a mesoporous material and has shown high photocatalytic activity in the degradation of 4-NP, indicating that CuPp manages to sensitize TiO_2. So it is conducive to the photodegradation of 4-NP.

2. Experiment

2.1. Materials and reagents

All the reagents and solvents were purchased from commercial sources and used without further purification except the pyrrole, which needed to be distilled before using.

2.2. Equipment

Mass spectrometry (MS) analyses were carried out on a matrix assisted laser desorption/ionization time of flight mass spectrometer (MALDI-TOF MS, Krato Analytical Company of Shimadzu Biotech, Manchester, Britain) using a standard procedure involving 1 mL of the sample solution. Elemental analyses (C, H and N) were performed by the Vario EL-III CHNOS instrument. UV-vis spectra were measured on a Shimadzu UV 1800 UV-vis-NIR spectrophotometer. Infrared spectra were measured on a Nicolet Avatar 330 FT-IR spectrometer with KBr pellets. The morphology of the sample by means of scanning electron microscopy (SEM) was analyzed (Quanta400FEG, mag. 200000×, HV 20.00kV, High vacuum, WD 11.5 mm, HFW 1.49 μm). High-resolution transmission electron microscopy (HRTEM) was carried out using a JEOL JEM-3010 instrument. The surface area was measured using the nitrogen adsorption-desorption isotherms. The pore diameter distribution curves of the samples were calculated using the pore size analyzer (Autosorb-1MP, Quantachrome, USA). The powder X-ray diffraction (XRD) measurement was performed with a Bruker D8 diffractometer using graphite monochromatic copper radiation (Cu K) at 40 kV, 30 mA over the 2θ range 20–70°. The UV-vis diffuse reflectance spectra (DRS) were recorded on a Shimadzu UV-3100 spectrophotometer by using $BaSO_4$ as a reference. A model XPA-VII photocatalytic reactor with a halogen lamp as the light source (Xujiang Electromechanical Plant, Nanjing, China) was employed to evaluate the degradation of 4-nitrophenol (4-NP).

2.3. Synthesis of (4-formyl-phenoxy)-acetic acid ethyl ester

The starting material (4-formyl-phenoxy)-acetic acid ethyl ester was prepared by

the reaction of 4-hydroxy-benzaldehyde and ethyl chloroacetate [16], which was in detail as follows: 12.2 g (0.1 mol) of 4-hydroxy-benzaldehyde was dissolved in 50 mL of acetone and mixed with 12 mL (0.1 mol) of ethyl chloroacetate with the presence of anhydrous potassium carbonate (13.8 g). They were refluxed at 65℃ for five to six hours. The procedure is as follow:

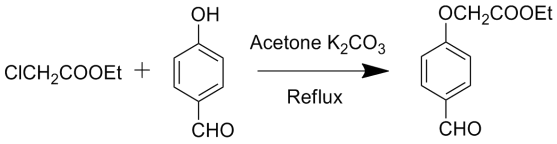

Scheme 1. The general route for (4-formyl-phenoxy)-acetic acid ethyl ester.

The mixture was then cooled down with ice water and kept for three hours. The white solid precipitation was filtered and washed with ice water several times. The crude product was recrystallized in ethanol. The crystal was then dried in a vacuum oven for six hours. Finally, a bright pale-yellow crystalline product was obtained.

Yield: 78 %. Mp: 34~39 °C. Anal. calcd. (found) for $C_{11}H_{12}O_4$ (Mol. Wt: 208.2), %: C 63.45 (63.46), H 5.81 (5.76).

2.4. Synthesis of porphyrin (H_2Pp-OEt) and metalloporphyrins (CuPp-OEt, CuPp)

The synthetic routes for porphyrin and metalloporphyrins are as follows:

Step 1

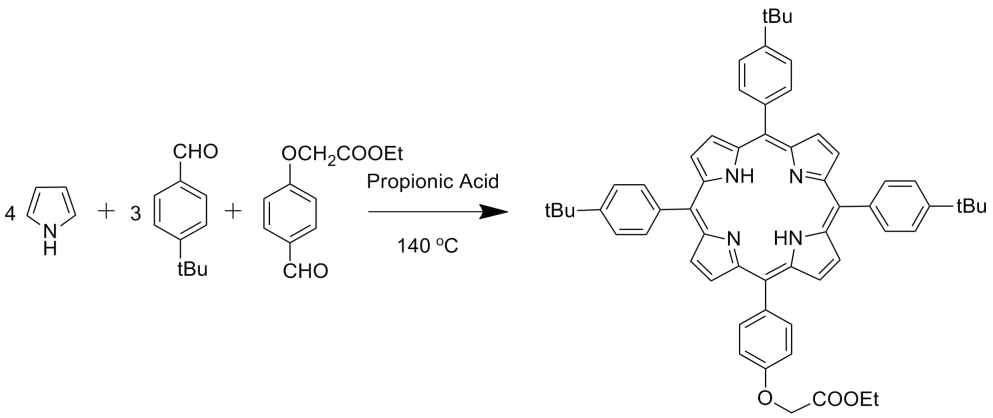

Step 2

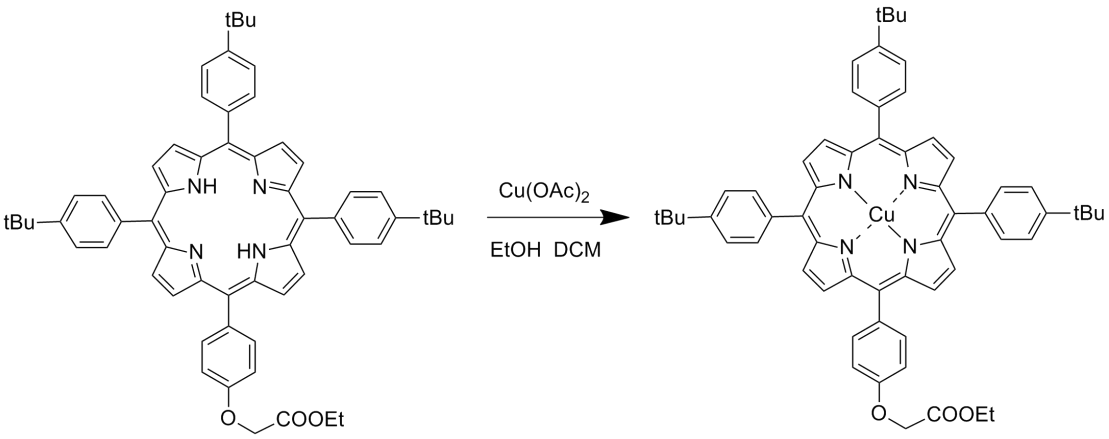

Step 3

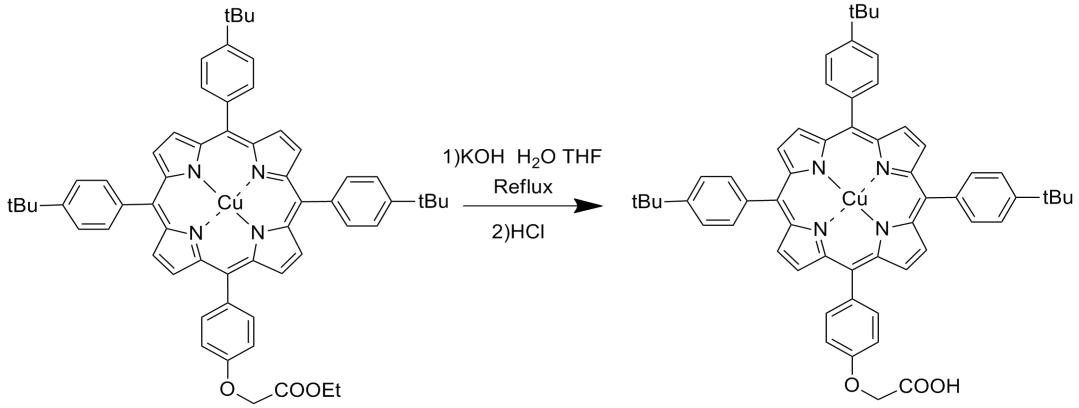

Scheme 2. The general routes for synthesizing porphyrin (H_2Pp-OEt) and metalloporphyrins (CuPp-OEt, CuPp).

2.4.1 Synthesis of (H_2Pp-OEt)

5[4-(carboethoxymethyleneoxy)phenyl]-10,15,20-tri(4-butylphenyl) porphyrin

The H_2Pp-OEt was prepared according to the literature [16]. 50 mL of propionic acid were refluxed at 140 °C for twenty minuets together with 4-*tert*-butylbenzaldehyde (7.65 mL, 45 mmol) and (4-formyl-phenoxy)-acetic acid ethyl ester (3.12 g, 15 mmol), which reacted with a molar ratio 3:1. Newly distilled pyrrole (4.2 mL, 60 mmol) in 15 mL of propionic acid was added dropwise over the course of thirty minutes. Then the mixture was vigorously stirred for an hour. Then the solvent was removed by the vacuum evaporation. After cooling down to room temperature, the crude product was obtained with 20 mL of EtOH added in. Further

purification was carried out by silica gel column chromatography. The elution of the column with dichloromethane (CH_2Cl_2) gave the purple solid.

Yield: 23 %. Mp: >250 °C, Anal. calcd. (found) for $C_{60}H_{60}N_4O_3$(Mol. Wt: 884.47), %: C 81.47 (81.46), H 6.84 (6.83), N 6.34 (6.33); MS： m/z 885.5 $[M+H]^+$ amu. UV-vis (CH_2Cl_2): λ_{max}/nm, UV-Vis (CH_2Cl_2) λ_{max}/nm: 418 (Soret band), 514 (Q_I), 549 (Q_{II}), 589 (Q_{III}), 644 (Q_{IV}). FT–IR (KBr) ν/cm^{-1}: 3446, 2960, 2360, 1745, 1608, 1466, 1270, 1197, 1078, 965, 804, 736.

2.4.2 Synthesis of (CuPp-OEt)

Cu(II)

5[4-(carboethoxymethyleneoxy)phenyl]-10,15,20-tri(4-butylphenyl)porphyrin

0.2 g (1 mmol) of $Cu(OAc)_2$ and 89 mg of the synthesized H_2Pp-OEt (0.1 mmol), were dissolved in 20 mL of C_2H_5OH and 30 mL of CH_2Cl_2 respectively. Then they were mixed up in the 150-mL round-bottom flask. The mixture was stirred at room temperature for eight hours. The solvent was removed by rotary evaporation. The crude product was further purified by silica gel column chromatography with CH_2Cl_2 as an eluent. Then the eluent was removed by rotary evaporation.After dried in an infrared oven，the red solid was obtained.

Yield: 94 %. Mp: >250 °C, Anal. calcd. (found) for $C_{60}H_{58}CuN_4O_3$ (Mol. Wt: 945.67), %: C 76.20 (76.12), H 6.18 (6.18), N 5.93 (5.92); MS: m/z 946.4 $[M+H]^+$ amu. UV–vis (CH_2Cl_2) λ_{max}/nm: 416 (S band), 541 (Q_I), 648 (Q_{IV}); FT–IR (KBr) ν/cm^{-1}: 3446, 2962, 2360, 1763, 1183, 1635, 999, 803.

2.4.3 Synthesis of (CuPp)

Cu(II)5[4-(carboxymethyleneoxy)phenyl]-10,15,20-tri[(4-butylphenyl) phenyl] porphyrin

The CuPp was obtained by the hydrolysis of CuPp-OEt in a KOH aqueous solution. 0.1 g of CuPp-OEt was dissolved in 20 mL of tetrahydrofuran (THF) with 40 mL of 2 mol·L^{-1} aqueous KOH added into. Then this mixture was refluxed at 80 °C for about five hours while being constantly stirred. Thin-layer chromatography (TLC)

was used to check the process of the reaction. The pH of the solution was adjusted to 3 using HCl (aq) after the reaction finished. The precipitate was filtered and washed with distilled water and then dried in a vacuum oven at 80 °C for twelve hours. The red solid was collected.

Yield: 89 %. Mp: >250 °C, Anal. calcd. (found) for $C_{58}H_{54}CuN_4O_3$ (Mol. Wt: 917.62), %: C 75.91 (75.83), H 5.93 (5.68), N 6.11 (6.10); MS: m/z 916.4 $[M-H]^-$ amu. UV–vis (DMF) λ_{max}/nm: 418 (S band), 540 (Q band); FT–IR (KBr) ν/cm^{-1}: 3446, 2962, 2360, 1738, 1641, 1107, 1001, 803, 669.

2.5. Preparation of mesoporous TiO_2

The mesoporous TiO_2 was prepared according to the literature [17]: it was synthesized with the usage of cetyltrimethyl ammonium bromide (CTMAB) which was served as a template under hydrothermal conditions.

2.6. Synthesis of CuPp-TiO_2 photocatalyst

Typical procedure of CuPp-TiO_2: CuPp (28.4 mg, 30 μmol) was dissolved in 2 mL of DMF. Then 1 g of TiO_2 was added slowly into the solution. The suspension was obtained after stirring and transferred to a 25 mL Teflon-lined autoclave. It was kept at 150 ℃ in an oven for 3 days. The obtained suspension was centrifuged to collect precipitate. It was washed with deionized water and ethanol for several times. Finally the sample was dried at 80℃ for four hours in a vacuum oven and CuPp-TiO_2 was obtained.

2.7. Photocatalytic activity test

Photocatalytic activities of CuPp-TiO_2 were evaluated by the photodegradation of 4-nitrophenol (4-NP) using a photocatalytic reactor under the irradiation of a halogen lamp at room temperature. 10 mg of the photocatalyst were added into the 4-NP aqueous solution (50 mL, 1×10^{-4} mol·L^{-1}), into which air was bubbled during the reaction. The suspension was stirred in the dark for thirty minutes to ensure the establishment of adsorption-desorption equilibrium between the photocatalyst and 4-NP. Then the suspension was irradiated with a 400 W halogen lamp for sixty

minutes. 4 mL of the sample were withdrawn every six minutes during the irradiation and the photocatalyst was separated from the suspension by centrifugation. The photodegradation process was measured by the characteristic absorption band of 4-NP at 317 nm using a UV–vis spectrophotometer.

2.8. Stability of photocatalyst test

The stability tests of CuPp-TiO_2 were carried out according to the same way as the 4-NP photodegradation. Repetitive experiments in the photocatalytic degradation of 4-NP were carried out by using similar experimental techniques (10 mL 4-NP solution, 25 °C, 2 mg photocatalyst, irradiated by a 400 W halogen lamp for sixty minutes). Catalysts for each test were collected by centrifugation and dried in a vacuum oven after every reaction cycle. The photodegradation process was measured by the characteristic absorption band of 4-NP at 317 nm using a UV–vis spectrophotometer.

3. Results and discussion

3.1. Synthesis of CuPp

The general procedure for CuPp was illustrated in **scheme 2**. The synthetic route for H_2Pp-OEt used in our study was the well-known Adler-Longo method. The porphyrin CuPp-OEt was obtained by porphyrin H_2Pp-OEt and $Cu(OAc)_2$ reacting in a CH_2Cl_2/C_2H_5OH solution with a 94 % yield. Alkaline hydrolysis of the as-prepared CuPp-OEt resulted in the formation of CuPp.

3.2. Characterization of CuPp

3.2.1. MS analysis

The mass spectra of H_2Pp-OEt, CuPp-OEt and CuPp were consistent with the values of positively charged $[M+H]^+$, and negatively charged $[M-H]^-$ adducts respectively.

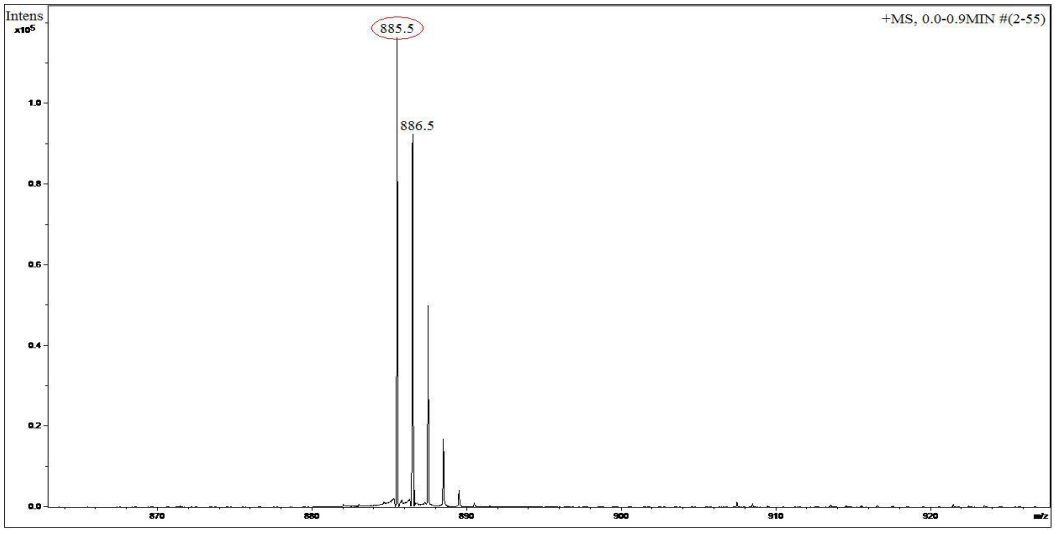

Fig. 1. MS spectrum of H_2Pp-OEt.

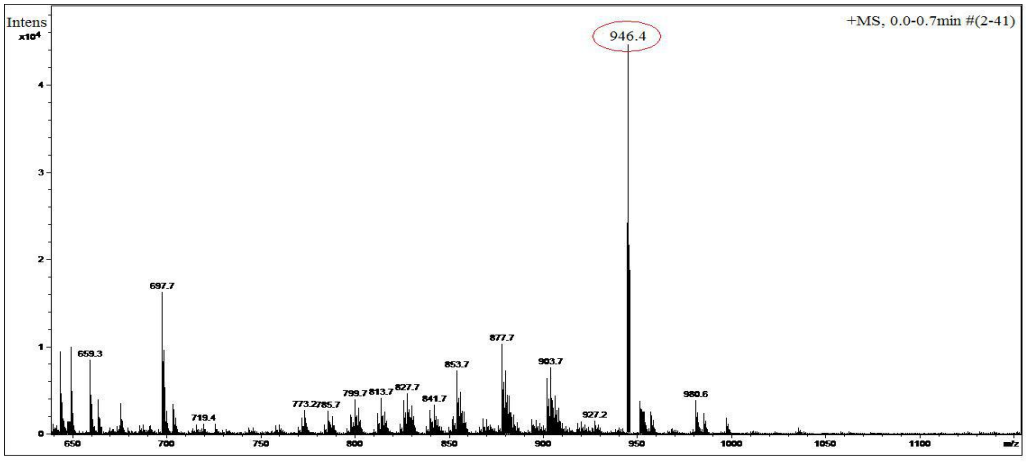

Fig. 2. MS spectrum of CuPp-OEt.

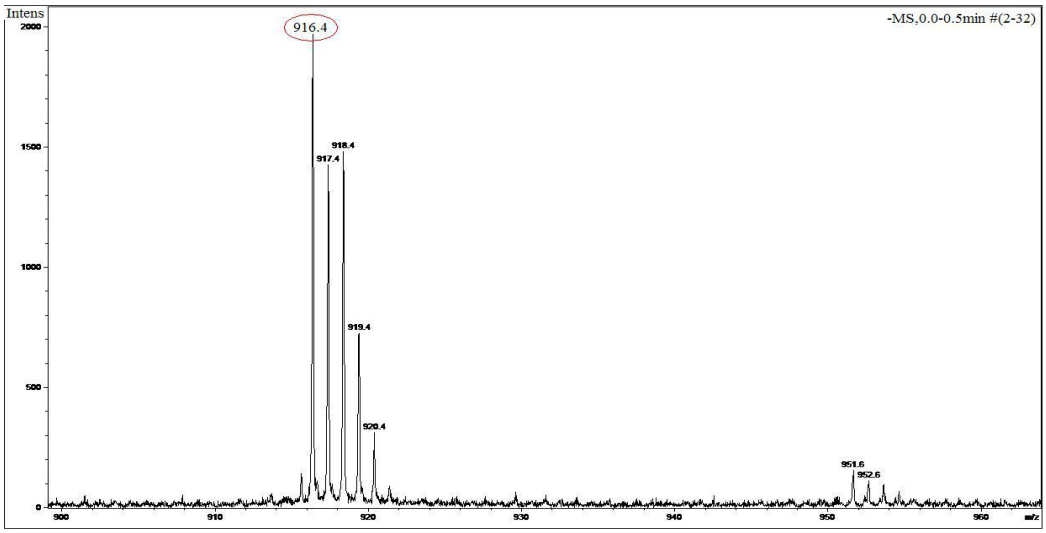

Fig. 3. MS spectrum of CuPp.

3.2.2. FT-IR analysis

The disappearance of N-H bending vibration at around 960 cm^{-1} in FT–IR spectra was attributable to the coordination of Cu(II) ions and N atoms in porphrins. The peak at 1740 cm^{-1} was assigned to symmetric ν^s(C=O) stretching vibration. The vibrations at around 1100 cm^{-1} and 1600, 1460 cm^{-1} were evinced by the $\nu^s_{Ar–O–C}$ stretching vibration and the $\nu^s_{C=O}$ benzene skeleton stretching vibration for aromatic groups.

Table 1. The FR-IR data of porphyrins.

porphyrins	δ_{N-H} vibration (cm^{-1})	$\nu^s_{Ar–O–C}$ Vibration (cm^{-1})	Benzene skeleton vibration (cm^{-1})	$\nu^s_{C=O}$ vibration (cm^{-1})	ν^{as}_{C-H} vibration (cm^{-1})
H_2Pp-OEt	961	1078	1608,1466	1745	2960
CuPp-OEt	---	1183	1635	1746	2962
CuPp	---	1107	1641	1738	2962

3.2.3. UV-vis analysis

The UV-vis spectra of copper porphyrins were characterized by Soret and Q bands. The number of Q bands decreased, because the symmetries of the porphyrins have increased with Cu(II) ions inserting in porphyrin rings [18]. The structure of the porphyrin synthesized here was well confirmed by the spectroscopic data.

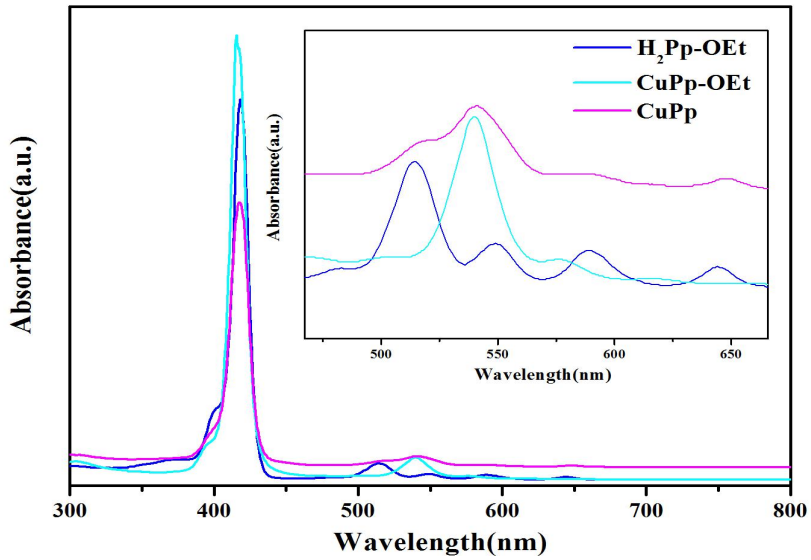

Fig. 4. UV–vis spectra of CuPp. The insertion is the fine structure of the Q bands.

3.3. Synthesis of CuPp-TiO_2

In order to make the reactants come into full contact, the one-pot solvothermal method was used to synthesize the CuPp-TiO_2 photocatalyst efficiently. And finally the powdery product was obtained.

3.4. Characterization of CuPp-TiO_2

3.4.1. SEM and TEM analysis

Fig. 5. (a) shows the SEM image of the CuPp-TiO_2 photocatalyst, where CuPp loads on the surface of TiO_2. It could be seen that the CuPp-TiO_2 particles are uniform nanospheres with mean diameters of ~30 nm. Numerous nanoparticles aggregate to form a spongiform arrangement, in which mesoporous are contained.

The high resolution transmission electron microscopy (HRTEM) image of CuPp-TiO_2 is illustrated in **Fig. 5. (b)**. Here exist two different kinds of lattice fringes in the CuPp-TiO_2 photocatalyst. The typical narrow fringes corresponded to the {101} planes of anatase TiO_2, indicating the nice crystallinity of TiO_2, while the wide fringes were consistent with the separate crystal planes of the CuPp.

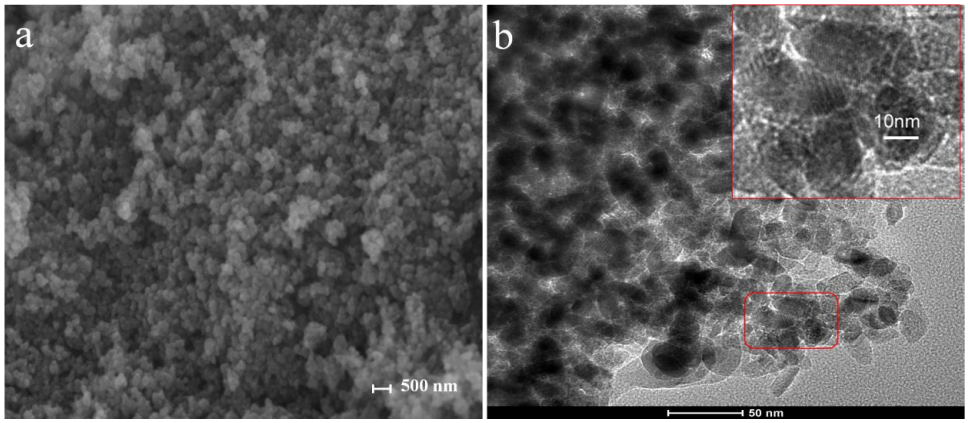

Fig. 5. SEM (a) and TEM (b) images of CuPp-TiO_2 photocatalyst. The insertion is the fine structure of CuPp-TiO_2 photocatalyst.

3.4.2. BET analysis

N_2 adsorption and desorption measurements were used to measure the specific surface area and porosity (**Fig. 6.**). Nitrogen adsorption-desorption isotherms were performed at 77.3 K. CuPp-TiO_2 photocatalyst exhibits a typical type IV isotherm with an H2-type hysteresis loop according to the IUPAC classifications, revealing an

uptake capacity of 128 $cm^3 \cdot g^{-1}$ for a mesoporous material [19]. The BET surface area for mesoporous CuPp-TiO_2 is 74.87 $m^2 \cdot g^{-1}$, which can be assigned to the pyknomorphic accumulation of nanoparticles. Besides, the pore size distribution of CuPp-TiO_2 is about 10 nm.

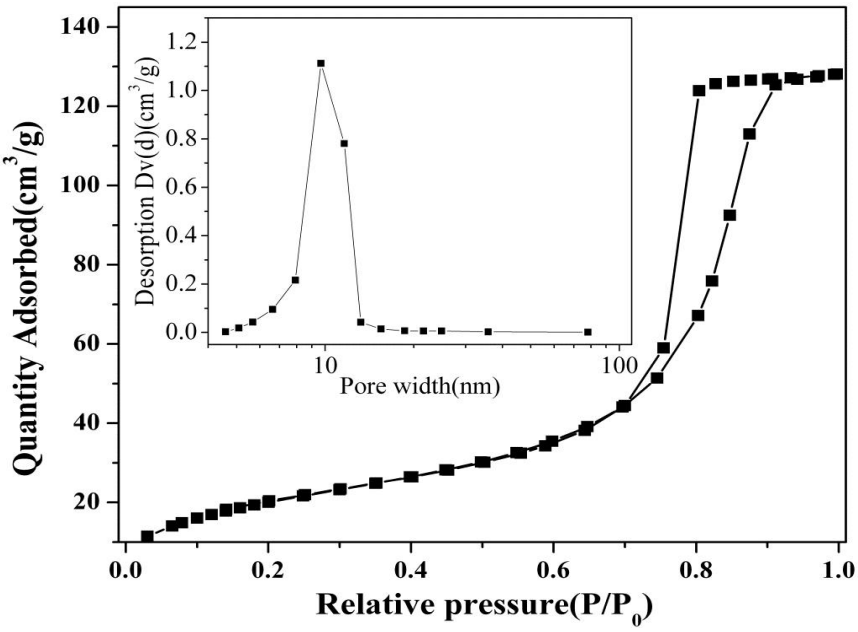

Fig. 6. N_2 adsorption and desorption isotherms of CuPp-TiO_2. The insertion is the pore size distribution of CuPp-TiO_2.

3.4.3. XRD analysis

Fig. 7. was the image of the XRD pattern for the CuPp-TiO_2 photocatalyst and bare TiO_2. The diffraction peaks corresponded to the characteristic peaks for anatase TiO_2 [20], i.e. the broadening XRD peaks of the anatase phase confirmed the nano nature of the TiO_2, which suggested that the CuPp loaded on the surface of TiO_2 would not change the intrinsic property (anatase phase) of the TiO_2, while only the crystallinity might be influenced.

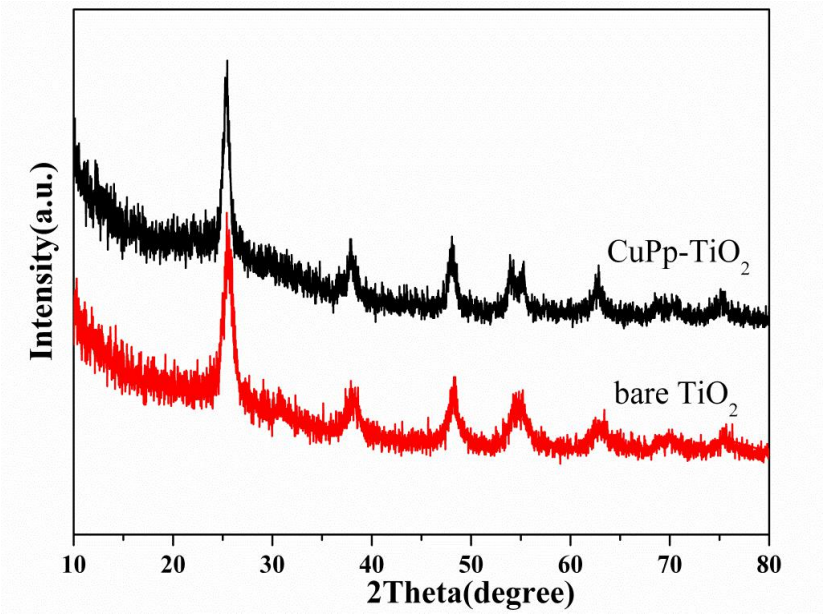

Fig. 7. XRD pattern of CuPp-TiO_2 photocatalyst and bare TiO_2.

3.4.4. FT-IR analysis

Table 2. shows the FT-IR spectral data of the porphyrin and the CuPp-TiO_2 photocatalyst. The absorption peak at around 3420 cm^{-1} was associated with the stretching vibration of the hydroxyl group, which was the –OH on the surface of TiO_2. The disappearance of C=O stretching vibration of the CuPp at around 1740 cm^{-1} and the appearance of a new band at around 1644 cm^{-1} in CuPp-TiO_2 might be attributed to the asymmetric stretch vibration of $–COO^-$, from which it could be concluded that CuPp was adsorbed on the surface of the TiO_2 by a chemical bond (Ti-O-C=O) and thus promotes the electron transfer between porphyrin molecules and Ti (3d) orbital. Due to the existence of C-O-Ti and C=O, it is easier to separate photogenerated electrons and holes, which greatly improves the photocatalytic activity of TiO_2.

Table 2. The FR-IR data of CuPp-TiO_2 photocatalyst.

Sample	$\nu^s_{Ar–O–C}$ Vibration (cm^{-1})	Benzene skeleton vibration (cm^{-1})	$\nu^s_{C=O}$ vibration（cm^{-1}）	ν^{as}_{C-H} vibration (cm^{-1})	δ_{C-H} vibration (cm^{-1})	Ti-O characteristic vibration (cm^{-1})	ν_{O-H} vibration (cm^{-1})	A new band (cm^{-1})
CuPp	1107	1641	1738	2962	803	---	---	---
CuPp-TiO_2	---	---	---	---	---	717	3220	1644

3.4.5. UV–vis–DRS analysis

UV–vis–DRS spectra of CuPp-TiO_2 and bare TiO_2 were measured and shown in **Fig. 8**. There was no apparent absorption in visible light range for bare TiO_2. While the characteristic absorption bands (the Soret and Q bands of CuPp), which were associated to the typical absorption bands for CuPp, were observed in the spectrum of the mesoporous photocatalyst CuPp-TiO_2 separately, indicating that the CuPp managed to sensitize the TiO_2 with the integrated porphyrin framework. As a result, CuPp-TiO_2 photocatalyst exhibited a broader absorption range in the solar spectrum than bare TiO_2.

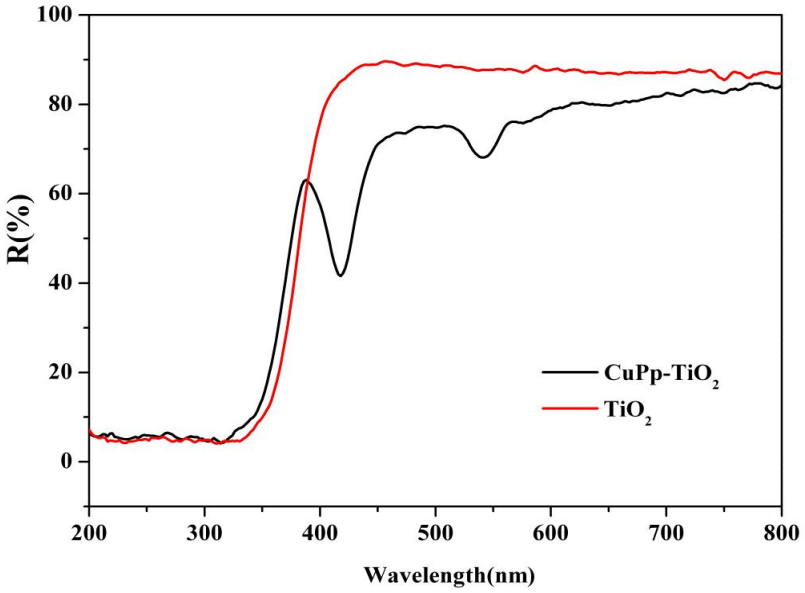

Fig. 8. UV–vis–DRS spectra of CuPp-TiO_2 photocatalyst and bare TiO_2.

3.4.6. Photocatalytic property of CuPp-TiO_2

4-nitrophenol (4-NP) was used to test the photocatalytic activity for CuPp-TiO_2 photocatalyst in the study. It could be seen in **Fig. 9.** that both TiO_2 and CuPp-TiO_2 photocatalysts could photodegrade 4-NP efficiently, while an increase of photocatalytic activity was observed on the CuPp-TiO_2 compared with bare TiO_2, because the loaded CuPp is beneficial for the photogenerated electrons transformation. And the CuPp-TiO_2 photocatalyst synthesized showed a higher photocatalytic activity than the previous report [15]. The photoactivity results indicate that the CuPp-TiO_2 photocatalyst synthesized is a potential candidate for organic pollutants

photodegradation.

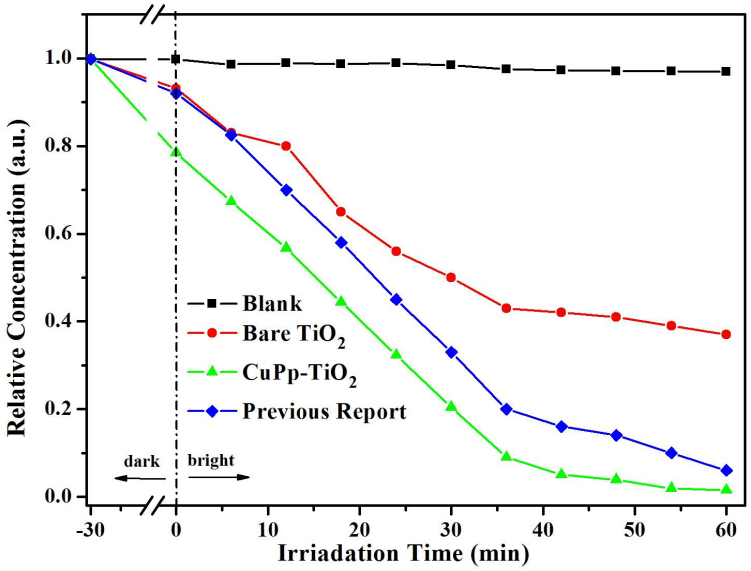

Fig. 9. Photodegradation of 4-nitrophenol (4-NP).

3.4.7. Stability of the CuPp-TiO_2 photocatalyst

In order to ensure that the CuPp-TiO_2 photocatalyst could be reused and chemically stable, the stability tests for CuPp-TiO_2 composite photocatalyst were carried out according to the same methods as the photodegradation of 4-NP. The catalytic efficiency was evaluated by the percentage of degraded 4-NP in sixty minutes. At the first cycle, nearly 100% 4-NP was degraded and the result was shown in **Fig. 10**. CuPp-TiO_2 prepared was marginally reduced to 98.4 %, 92.3 %, 87.4 %, 81.2 %, 77.5 % after every respective experimental cycle (six times in total), which exhibited a better stability than the previous report [15], indicating the relatively higher stability of this photocatalyst. Furthermore, the CuPp-TiO_2 photocatalyst could be simply recycled by centrifugation, which makes it an environmentally friendly way to treat polluted water. It confirmed that the CuPp loaded on the surface of TiO_2 displayed remarkable stability under irradiation.

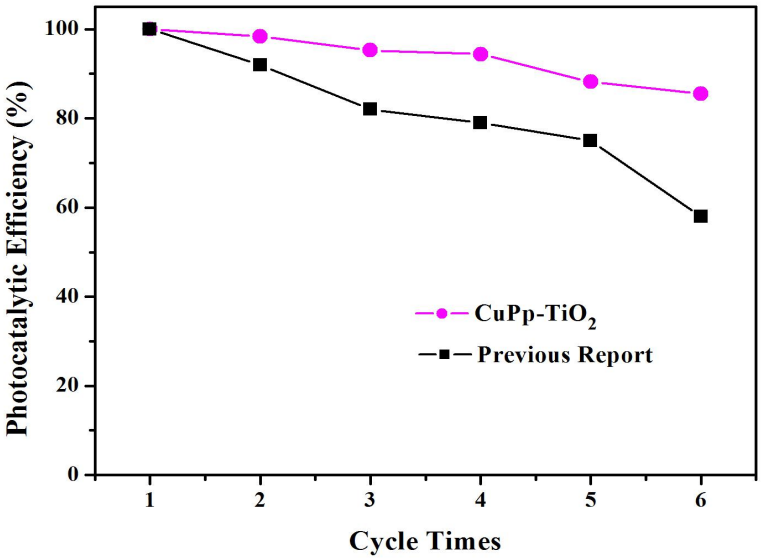

Fig. 10. Stability tests of the CuPp-TiO_2 photocatalyst.

4. Conclusion

In this research, a novel copper porphyrin has been designed and synthesized. And the one-pot solvothermal method has been applied to synthesize the CuPp-TiO_2 photocatalyst. All the spectroscopic characterizations have evidenced the structure of the compounds we fabricated. The SEM, TEM, BET, XRD and UV–vis–DRS analyses for the CuPp-TiO_2 photocatalyst have proved that the presence of CuPp would not change the crystal structure of the TiO_2, while it only interlinks with the surface of TiO_2 and improves the photocatalytic properties successfully. The CuPp-TiO_2 photocatalyst we prepared exhibits better photoactivity and higher stability under visible light irradiation than pure TiO_2 and the previous report in the photodegradation of 4-NP test. So it would be a promising material in organic pollutant treatments.

5. Acknowledgements

We deeply appreciate those who have helped us during this research, especially Professor Li in Northwest University, Xi'an.

We thank her for kindly providing our equipment and reagents and also for her helpful advice in the writing of our thesis and the spectra analyses.

References

[1] Gavrilescu M, Demnerová K, Aamand J. Emerging pollutants in the environment: present and future challenges in biomonitoring, ecological risks and bioremediation. *New biotechnology*, **2015**, 32(1)，147–156

[2] Lyu J, Zhu L, Burda C. Considerations to improve adsorption and photocatalysis of low concentration air pollutants on TiO_2. *Catalysis Today*, **2014**, 225, 24–33

[3] Huang C, Lv Y, Zhou Q, Kang S, Li X, Mu J. Visible photocatalytic activity and photoelectrochemical behavior of TiO_2 nanoparticles modified with metal porphyrins containing hydroxyl group. *Ceramics International*, **2014**, *40*, 7093–7098

[4] Bleta R, Lannoy A, Machut C, Monflier E, Ponchel Anne. Understanding the role of cyclodextrins in the self-assembly, crystallinity, and porosity of titania nanostructures. *Langmuir*, **2014**, *30*, 11812−11822

[5] Mondal K, Bhattacharyya S, Sharma A. Photocatalytic degradation of naphthalene by electrospun mesoporous carbon-doped anatase TiO_2 nanofiber mats. *Ind. Eng. Chem. Res.*, **2014**, *53*, 18900–18909

[6] Mele G, Annese C, D'Accolti L, Riccardis A, Fusco C, Palmisano L, Scarlino A and Vasapollo G. Photoreduction of carbon dioxide to formic acid in aqueous suspension: A comparison between phthalocyanine/TiO_2 and porphyrin/TiO_2 catalysed processes. *Molecules*, **2015**, *20*, 396-415

[7] Ma Y, Wang X, Jia Y, Chen X, Han H, Li C. Titanium dioxide-based nanomaterials for photocatalytic fuel generations. *Chem. Rev.*, **2014**, 114, 9987−10043

[8] Singh K, Nowotny J, Thangadurai V. Amphoteric oxide semiconductors for energy conversion devices: a tutorial review. *Chem. Soc. Rev.*, **2013**, 42(5),1961-1972

[9] Chen H, Jin H, Dong B. Preparation of magnetically supported chromium and sulfur co-doped TiO_2 and use for photocatalysis under visible light. *Res. Chem. Intermed*, **2012**, 38, 2335–2342

[10] Yang Y, Zhong H, Tian C. Photocatalytic mechanisms of modified titania under visible light. *Res. Chem. Intermed*, **2011**, 37, 91–102

[11] Li W, Liu Z, Wu H, Cheng Y, Zhao Z, He H. Thiophene-functionalized porphyrins: Synthesis, photophysical properties, and photovoltaic performance in dye-sensitized solar cells. *J. Phys. Chem. C*, **2015**, 119, 5265–5273

[12] Lu Z, Liang M, Dai P, Miao K, Zhang C, Sun Z, Xue. A strategy for enhancing the performance of borondipyrromethene dye-sensitized solar cells. *J. Phys. Chem. C*, **2016**, 120 (45), 25657–25667

[13] Zhao X, Yuan L, Zhang Z, Wang Y, Yu Q, and Li J. Synthetic methodology for the fabrication of porous porphyrin materials with metal−organic−polymer aerogels. *Inorg. Chem.*, **2016**, 55(11)

[14] Sun Wan, Li J, Mele G, Zhang Z, Zhang F. Enhanced photocatalytic degradation of rhodamine B by surface modification of ZnO with copper (II) porphyrin under both UV–vis and visible light irradiation. *Journal of Molecular Catalysis A: Chemical*, **2013**, 366, 84–91

[15] Mi-mi Yu, Jun Li, Wan-jun Sun , Min Jiang, Feng-xing Zhang. Preparation, characterization, and photocatalytic properties of composite materials of copper(II) porphyrin/TiO_2. *Journal of Materials Science*, **2014**, 49(16), 5519-5528

[16] Duncan T.V., Wu S.P., Therien M.J. Ethyne-bridged (porphinato) Zinc(II)-(porphinato) Iron(III) complexes: phenomenological dependence of excited-state dynamics upon (porphinato) Iron electronic structure. *Journal of the American Chemical Society*, **2006**, (128), 10423-10435

[17] Adel A. Ismail and Detlef W. Bahnemann, Mesoporous titania photocatalysts: preparation, characterization and reaction mechanisms. *J. Mater. Chem.*, **2011**, 21, 11686–11707

[18] Giovannetti R. The Use of Spectrophotometry UV-Vis for the Study of porphyrins. *Macro To Nano Spectroscopy*, **2012**, 87-108

[19] Groen J, Peffer L, Pérez-Ramírez J. Pore size determination in modified micro- and mesoporous materials. Pitfalls and limitations in gas adsorption data analysis. *Micropor. Mesopor. Mat.*, **2003**, 60, 1－17

[20] Zhou P, Yu J, Jaroniec M. All‐Solid‐State Z‐Scheme photocatalytic systems. *Advanced Materials*, **2014**, 26(29), 4920-4935